Heterogeneous & Homogeneous & Bio- & Nano-
CHEMCATCHEM
CATALYSIS

Supporting Information

Correlative Multiscale 3D Imaging of a Hierarchical Nanoporous Gold Catalyst by Electron, Ion and X-ray Nanotomography

Yakub Fam,[a] Thomas L. Sheppard,*[a, b] Ana Diaz,[c] Torsten Scherer,[d] Mirko Holler,[c] Wu Wang,[d] Di Wang,[d] Patrice Brenner,[e] Arne Wittstock,[f] and Jan-Dierk Grunwaldt[a, b]

cctc_201800230_sm_miscellaneous_information.pdf
cctc_201800230_sm_FIB-SEM-CT_Movie.mpg
cctc_201800230_sm_PXCT_Movie.mpg

Author Contributions

Y.F. Conceptualization: Supporting; Formal analysis: Equal; Investigation: Lead; Methodology: Supporting; Project administration: Supporting; Validation: Equal; Visualization: Equal; Writing – original draft: Equal; Writing – review & editing: Supporting
T.S. Conceptualization: Equal; Formal analysis: Equal; Funding acquisition: Supporting; Investigation: Supporting; Methodology: Supporting; Project administration: Lead; Supervision: Equal; Validation: Equal; Visualization: Equal; Writing – original draft: Equal; Writing – review & editing: Lead
A.D. Data curation: Lead; Formal analysis: Supporting; Investigation: Supporting; Methodology: Equal; Resources: Supporting; Software: Equal; Validation: Supporting; Visualization: Supporting; Writing – review & editing: Supporting
T.S. Formal analysis: Supporting; Investigation: Supporting; Resources: Supporting; Writing – review & editing: Supporting
M.H. Data curation: Supporting; Formal analysis: Supporting; Investigation: Supporting; Methodology: Equal; Resources: Supporting; Software: Equal; Validation: Supporting; Visualization: Supporting; Writing – review & editing: Supporting
W.W. Formal analysis: Supporting; Investigation: Supporting; Resources: Supporting; Software: Supporting; Visualization: Supporting; Writing – review & editing: Supporting
D.W. Formal analysis: Supporting; Investigation: Supporting; Resources: Supporting; Software: Supporting; Visualization: Supporting; Writing – review & editing: Supporting
P.B. Formal analysis: Supporting; Investigation: Supporting; Resources: Supporting; Software: Supporting; Visualization: Supporting; Writing – review & editing: Supporting
A.W. Investigation: Supporting; Resources: Supporting; Writing – review & editing: Supporting
J.G. Conceptualization: Equal; Funding acquisition: Lead; Methodology: Supporting; Project administration: Supporting; Supervision: Equal; Writing – original draft: Supporting; Writing – review & editing: Supporting.

S1 - Sample Preparation

S2 - Ptychographic X-ray Computed Tomography (PXCT)

S3 - FIB-SEM Slice and View Tomography (FIB-SEM-CT)

S4 - Electron Tomography (ET)

S5 - Image Processing and Label Analysis

S6 - Pore Segmentation

S7 - Calculation of specific surface area (S) and pore volume (V_p)

S8 - Estimated Spatial Resolution of Tomographic Imaging Techniques

S9 - Supplementary Movie Files

S1 - Sample Preparation

All samples used in this work derived from a single piece of monolithic ceria-doped nanoporous gold (CeO_x/np-Au). From this piece, various samples were extracted for analysis by ET, PXCT and FIB-SEM-CT as outlined in Figure S1. All sample preparation steps were performed in a FIB Strata 400S (FEI Company, USA). The monolithic CeO_x/np-Au sample was firstly mounted on an SEM sample holder stub **(1)** (Figure S2), then cut and shaped with a Ga^+ ion beam to meet the sample requirements for ET **(2)** (Figure S3) and PXCT **(3)** (Figure S4). The remaining sample on the stub was retained for FIB-SEM-CT **(4)** (Figure S5).

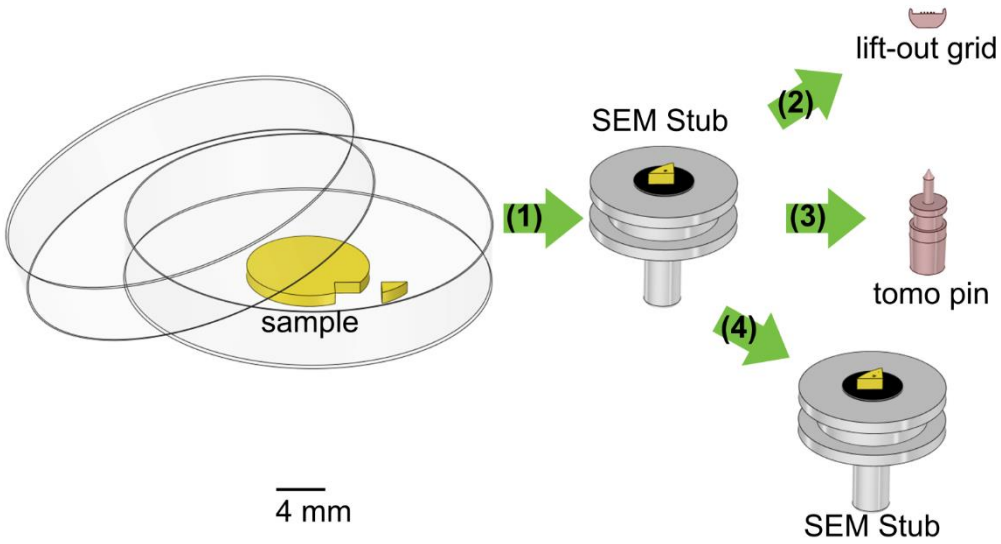

Figure S1. Overview of CeO_x/np-Au sample preparation for ET, PXCT, and FIB-SEM-CT.

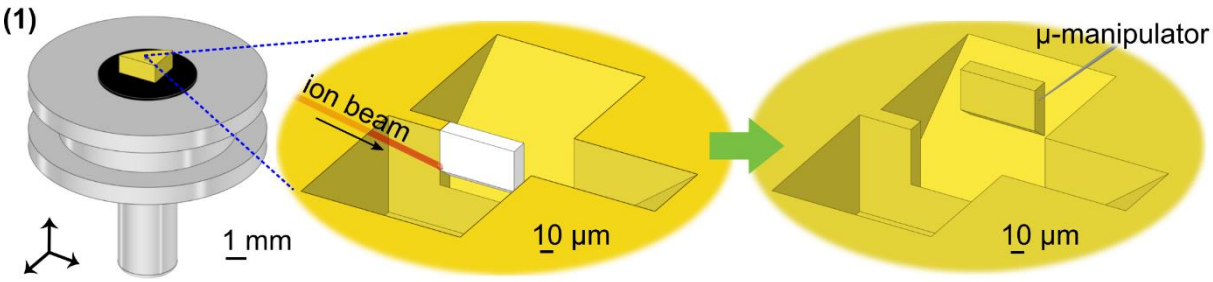

Figure S2. Monolithic CeO_x/np-Au was mounted on a stub and cut by Ga^+ beam. A small piece of material was extracted by FIB manipulation. This corresponds to procedure **(1)** in Figure S1.

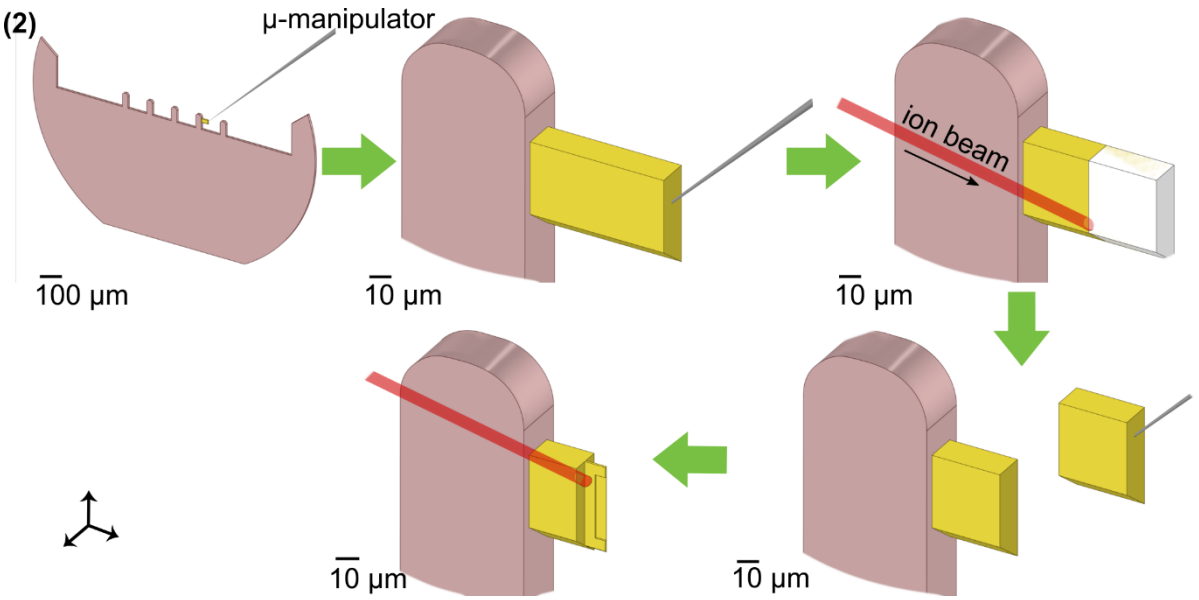

Figure S3. The CeO_x/np-Au piece extracted from the stub was moved to a lift-out grid by FIB manipulation. This piece was then thinned down by Ga^+ beam to <300 nm thickness for ET measurement. This corresponds to procedure **(2)** in Figure S1.

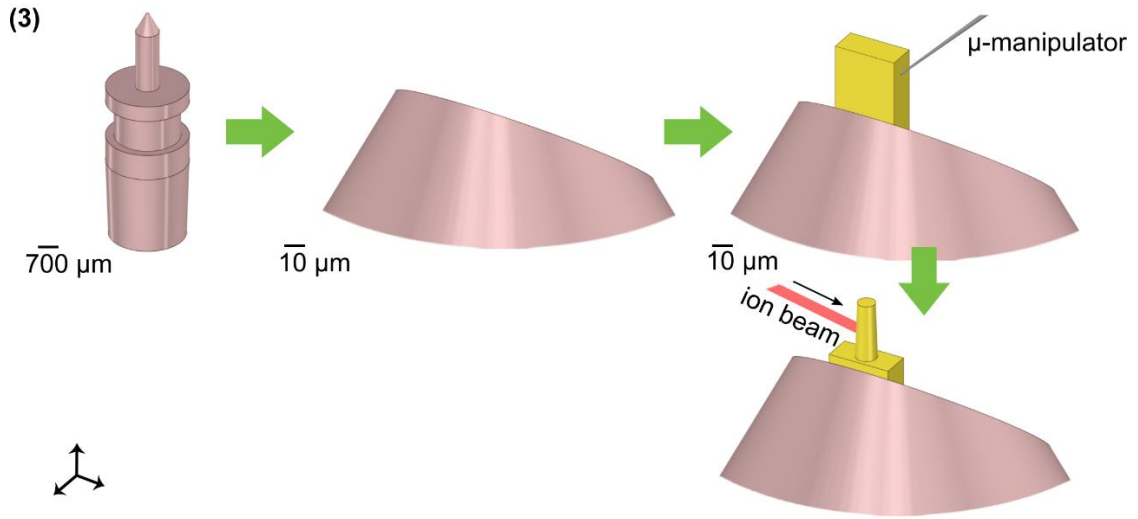

Figure S4. (Left) Customized Cu pin developed at cSAXS beamline (Swiss Light Source)[1]; (Middle-Right) a small piece of CeO_x/np-Au from the lift-out grid was moved to the Cu pin by FIB manipulation, which was then cut into a cylindrical shape for PXCT measurement. This corresponds to procedure **(3)** in Figure S1.

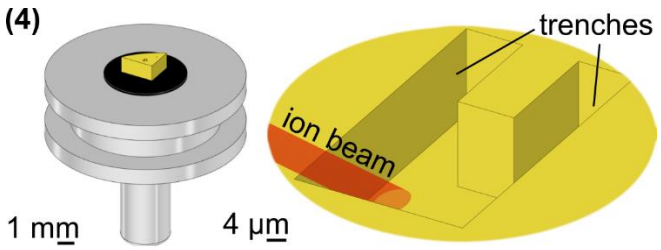

Figure S5. The remaining CeO_x/np-Au on the stub (Figure S2) was cut into a rectangular prism by Ga^+ beam for FIB-SEM-CT measurement. This corresponds to procedure **(4)** in Figure S1.

S2 - Ptychographic X-ray Computed Tomography (PXCT)

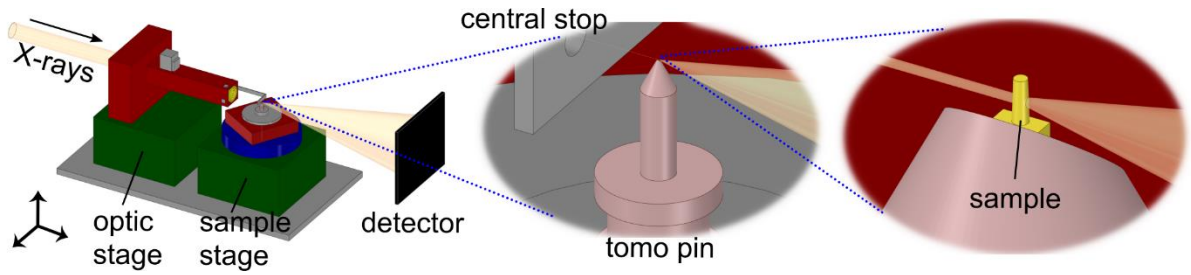

Figure S6. Illustration of PXCT setup at the cSAXS beamline (Paul Scherrer Institute, Switzerland).

S3 - FIB-SEM Slice and View Tomography (FIB-SEM-CT)

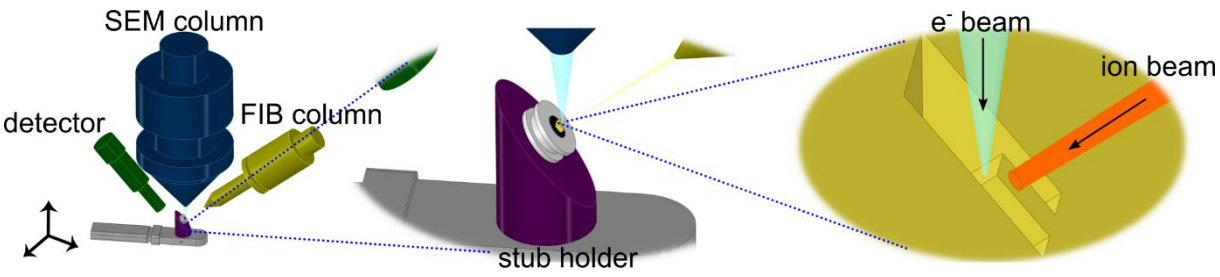

Figure S7. Illustration of FIB-SEM-CT setup at the Laboratory of Electron Microscopy (Karlsruhe Institute of Technology, Germany).

S4 - Electron Tomography (ET)

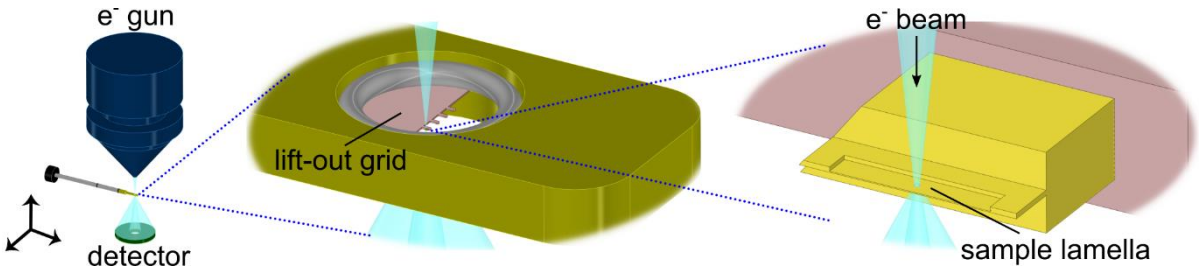

Figure S8. Illustration of ET setup at the Institute of Nanotechnology (Karlsruhe Institute of Technology, Germany).

S5 - Image Processing and Label Analysis

Images were rendered using Avizo 9.3 software (FEI). Default settings were applied for each data treatment module unless otherwise stated.

PXCT: TIFF images of 551 slices of cylindrical CeO_x/np-Au were used as the image source in Avizo, which were combined into a single volume with isotropic voxel size of 13.3 nm. A 'Non-Local Means Filter' module was employed to remove data noise. The filtered file was segmented into three bodies: CeO_x/np-Au, pores, and the central void. Exterior voxels including surrounding air and 2D frame padding were discarded using a circular binary mask. 'Threshold' tool was firstly used to approximately define CeO_x/np-Au and pores. Next,

'Watershed' tool was used to automatically compute a suitable contrast gradient between the selected np-Au and pore histogram values with the help of generated gradient image. 'Brush' tool was employed to roughly assign the central void volume. The segmentation was interpolated every 50 slices, followed by 'Watershed' to finalize the results. Finally, 'Lasso' tool was used to distinguish between exterior and pore voxels. Pores and CeOx/np-Au were then visualized individually in 3D via 'Volume Rendering' module. To obtain the values of volume (V) and surface area (S), 'Label Analysis' module with 3D interpretation was used. Further analysis to show np-Au ligament and pore size distribution was carried out using 'Separate Objects' module, followed by 'Label Analysis' module with customized measurement parameters to calculate equivalent diameter as the ligament or pore size.

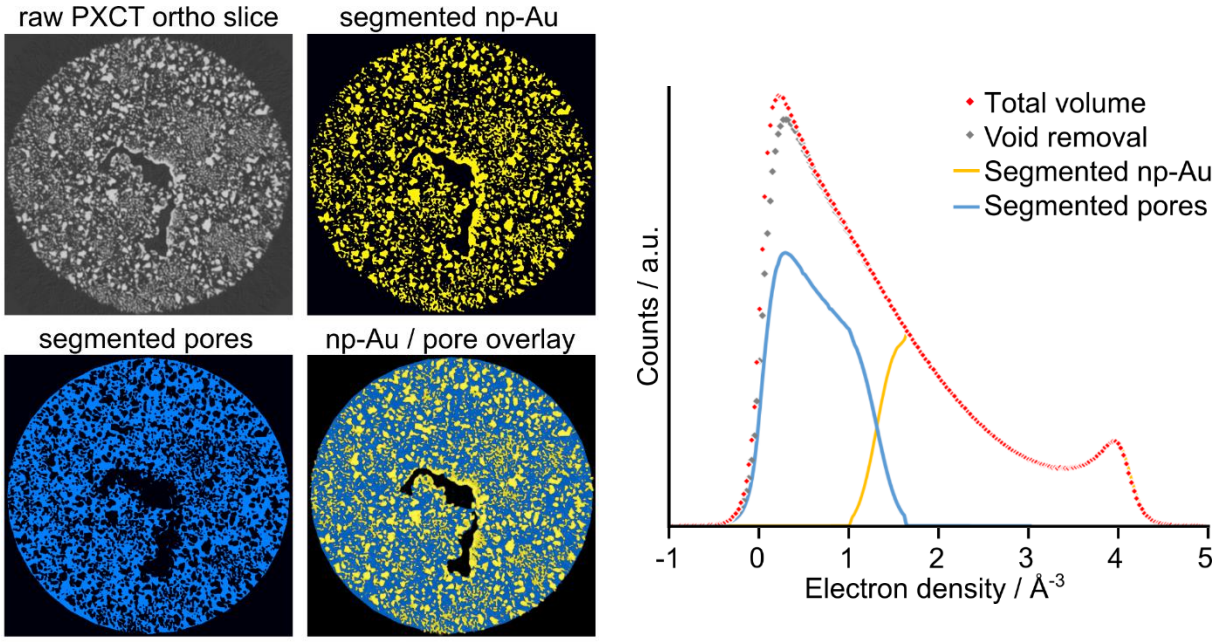

Figure S9. Example of segmentation procedure demonstrated on a single 2D orthographic sample slice derived from the 3D sample volume following ptychographic reconstruction. The respective electron density values and threshold parameters for removal of the central void, and watershed/threshold segmentation of np-Au and pores are also shown. Overlay image layers are shown with 75% transparency.

FIB-SEM-CT: TIFF images of 750 slices of box-like CeO_x/np-Au were used as the image source in Avizo, which were combined into a single volume with isotropic voxel size of 12.9 nm. A 'Non-Local Means Filter' module was employed to remove data noise. The filtered image stack required alignment, so 'FIB Stack Wizard' module was employed. Least-squares method was adopted in this case and the produced slices were then cropped, so that the material body was visible in all slices. Shear angle was set to 36° so as to correct the viewing angle of 54° during measurement. The aligned image stack was segmented into two bodies: CeO_x/np-Au and pores. Exterior voxels were discarded. 'Threshold' tool was firstly used to approximately define CeO_x/np-Au and pores. Next, 'Watershed' tool was used to automatically cover the missing areas with the help of generated gradient image. 'Lasso' tool was used to distinguish between exterior and pores on the first and last slices, whereas the rest of the slices were carried out by interpolation. Due to the shearing correction during alignment, the segmented volume was manipulated onto Cartesian axes using 'Resample Transformed Image' module. Each segmented body was then visualized in 3D via 'Volume Rendering' module. To obtain the values of volume (V) and surface area (S), 'Label Analysis' module with 3D interpretation was used. Further analysis to show np-Au ligament and pore size distribution was carried out using 'Separate Objects' module, followed by 'Label Analysis' module with customized measurement parameters to calculate equivalent diameter as the ligament or pore size.

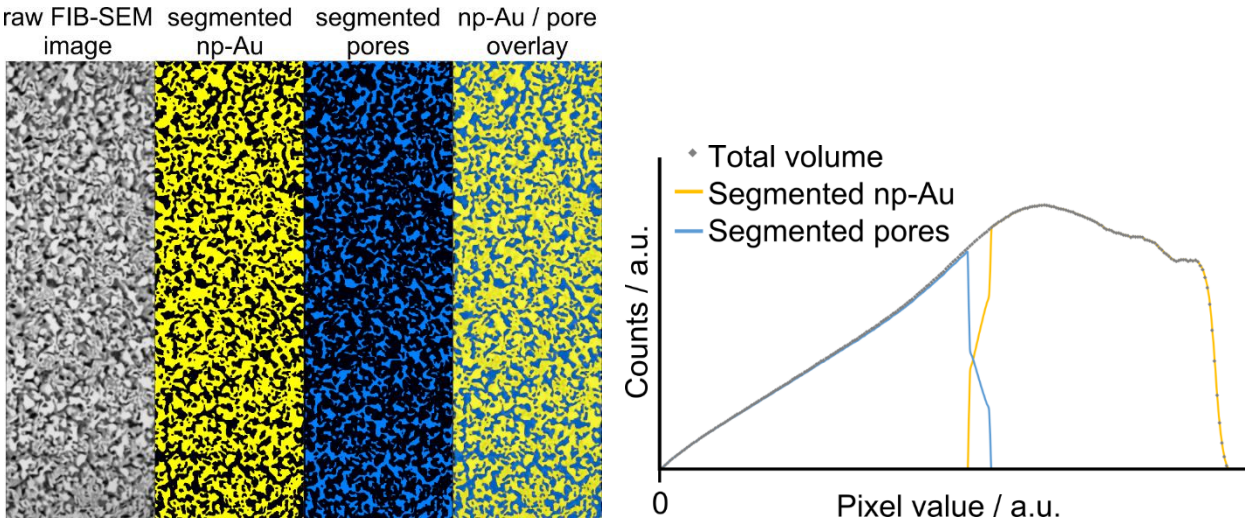

Figure S10. Example of segmentation procedure demonstrated on a single 2D SEM image produced during FIB-SEM cutting of the bulk sample. The respective histogram values and threshold parameters for segmentation of np-Au and pores are also shown. Overlay image layers are shown with 75% transparency.

ET: A single REC file containing lattice info of the CeO_x/np-Au lamella was used as the image source in Avizo. The isotropic voxel size was set to 1.3 nm. A 'Non-Local Means Filter' module was employed to remove data noise. The filtered file was segmented into two bodies: CeO_x/np-Au and pores. Exterior voxels were discarded. 'Threshold' tool was firstly used to approximately define CeO_x/np-Au and pores. Next, 'Blow', 'Brush' and 'Interpolate' tools were employed to manually distinguish each part. Each segmented body was then visualized in 3D via 'Volume Rendering' module. To obtain the values of volume (V) and surface area (S), 'Label Analysis' module with 3D interpretation was used. Further analysis to show np-Au ligament and pore size distribution was carried out using 'Separate Objects' module, followed by 'Label Analysis' module with customized measurement parameters to calculate equivalent diameter as the ligament or pore size.

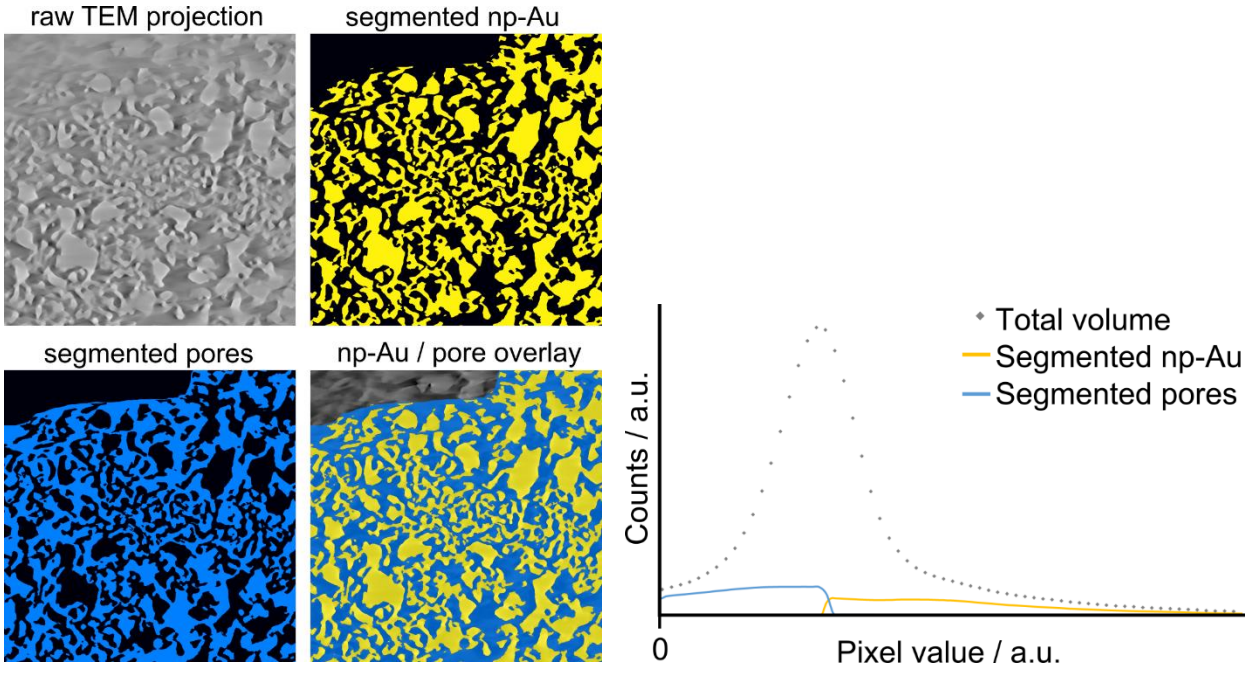

Figure S11. Example of segmentation procedure demonstrated on a single 2D TEM projection representing one tilt angle. The respective histogram values and threshold parameters for segmentation of np-Au and pores are also shown. Overlay image layers are shown with 75% transparency. Note the upper left area was discarded due to poor contrast.

Label Analysis: 'Label Analysis' module with 3D interpretation was used to obtain several values of 'Volume3d', representing the corresponding segmented volume (see Volume in Table 2) and 'Area3d' representing the corresponding segmented surface area (see Area in Table 2). Further analysis to show the size distributions of np-Au ligament and pore was carried out using the 'Separate Objects' module to cut the continuous volume structure into individual subunits (Figure S12). This was followed by 'Label Analysis' module with customized measurement parameters to calculate 'Equivalent Diameter' as the ligament or pore size of each subunit with the following formula:

$$Equivalent\ Diameter = \sqrt[3]{\frac{6 * Volume3d}{\pi}}$$

From the resulting pore size distribution values, further calculation of pore sphericity was also applied using the following formula, derived from Wadell et al:[2]

$$Pore\ Sphericity = \frac{\pi^{\frac{1}{3}} * (6 * Volume3d)^{\frac{2}{3}}}{A}$$

Volume3d = volume of the object, A = surface area of the object. The above equation represents the ratio of the surface area of a sphere (with the same volume as the object of interest) to the surface area of the subunit being measured after object separation. A sphere has pore sphericity value of 1, objects deviating from this value as regarded as progressively less spherical. The average of such distributed values (see Average Pore Sphericity in Table 1) is versatile enough to generally show how spherical the segmented pore is for each technique. It should be noted that approximating pores to spheres is only one method of pore volume analysis. By applying this consistently for all three nanotomography techniques, any errors resulting from the measurement should be proportional for all three techniques.

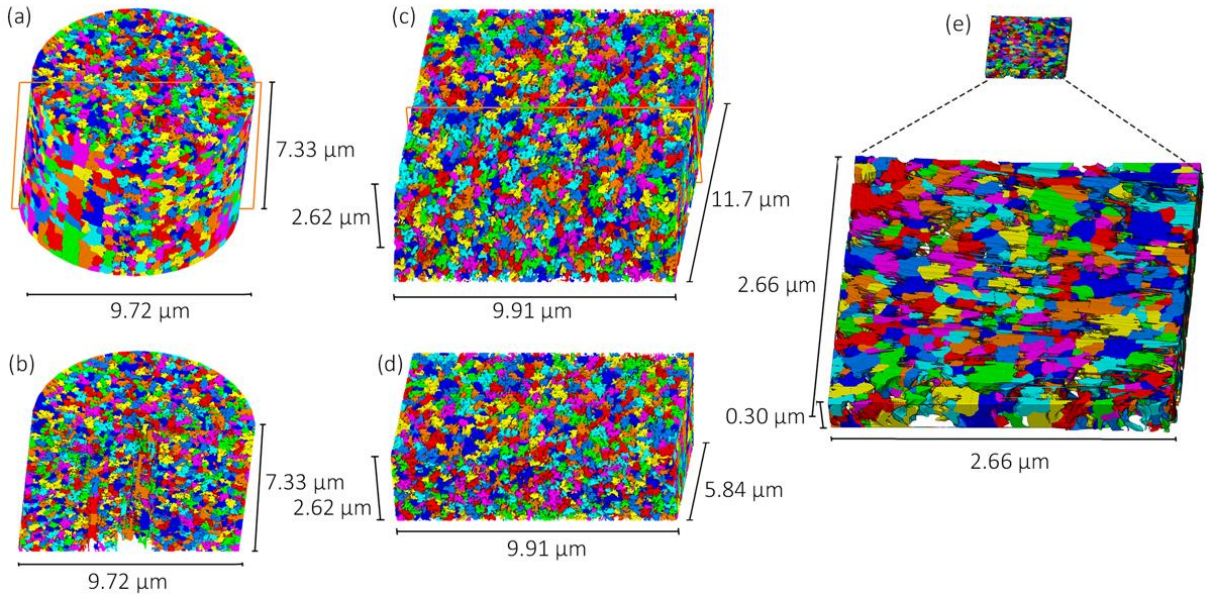

Figure S12. Label analysis of (a) whole and (b) bisected CeO_x/np-Au cylinder via PXCT; (c) whole and (d) bisected CeO_x/np-Au cuboid via FIB-SEM-CT; (e) CeO_x/np-Au lamella to scale (above) and magnified (below) as observed via ET. Cutting planes indicated by red lines.

S6 - Pore Segmentation

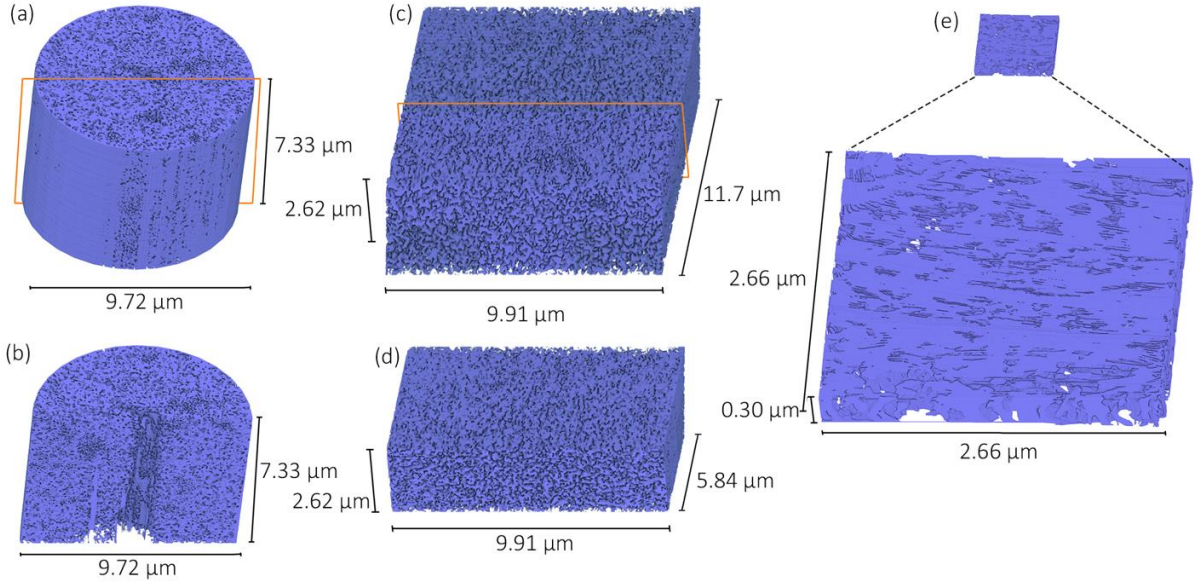

Figure S13. Volume rendering of (a) whole and (b) half-cut pore of cylindrical CeO_x/np-Au via PXCT; (c) whole and (d) half-cut pore of rectangular-prismic CeO_x/np-Au via FIB-SEM-CT; whole and magnified thin-layered pore of CeO_x/np-Au via ET.

S7 – Calculation of specific surface area (S) and pore volume (V_p)

In the following formulae, material *A* and material *B* denote either np-Au or CeO_2 interchangeably. The mass percentage data of CeO_x/npAu was derived from TEM-EDX measurements. Volume data was acquired directly by voxel counting of the 3D volumes. Since the density of CeOx/npAu ($\rho_{mix} = \rho_{/(CeOx/npAu)}$) is one of the required variables to obtain the value of specific surface area (S), and the density of pure Au and/or CeO_2 are known, the following equation can then be derived:

$$\%w_A = \frac{m_A}{m_{mix}} = \frac{\rho_A * V_A}{\rho_{mix} * V_{mix}} = \frac{\rho_A}{\rho_{mix}} * \frac{V_A}{V_{mix}} = \frac{\rho_A * \%v_A}{\rho_{mix}}$$

$$\rho_A = \frac{\%w_A * \rho_{mix}}{\%v_A}$$

However, "$\%v_A$" variable here is unknown, so another equation is required to correlate $\%v_A$ to an inherently known sample parameter (i.e. mass) with the following equation:

$$\%v_A = \frac{V_A}{V_{mix}} = \frac{V_A}{V_A + V_B} = \frac{\frac{V_A}{m_{mix}}}{\frac{V_A}{m_{mix}} + \frac{V_B}{m_{mix}}} = \frac{\frac{m_A}{m_A} * \frac{V_A}{m_{mix}}}{\frac{m_A}{m_A} * \frac{V_A}{m_{mix}} + \frac{m_B}{m_B} * \frac{V_B}{m_{mix}}} = \frac{\frac{\frac{m_A}{m_{mix}}}{\frac{m_A}{V_A}}}{\frac{\frac{m_A}{m_{mix}}}{\frac{m_A}{V_A}} + \frac{\frac{m_B}{m_{mix}}}{\frac{m_B}{V_B}}}$$

$$\%v_A = \frac{\frac{\%w_A}{\rho_A}}{\frac{\%w_A}{\rho_A} + \frac{\%w_B}{\rho_B}}$$

Annotations:

$m = mass$
$\rho = density$
$V = volume$
$\%v = volume\ fraction$
$\%w = mass\ fraction$
$S = specific\ surface\ area$
$V_P = pore\ volume$

The first (highlighted in blue) and second equation (highlighted in yellow) are combined to eventually obtain the value of $\rho_{/(CeOx/npAu)}$:

$$\%v_{Au} = \frac{\frac{\%w_{Au}}{\rho_{Au}}}{\frac{\%w_{Au}}{\rho_{Au}} + \frac{\%w_{CeOx}}{\rho_{CeOx}}}$$

$$\rho_{Au} = \frac{\%w_{Au} * \rho_{CeOx/npAu}}{\%v_{Au}}$$

$$\rho_{CeOx/npAu} = \frac{\rho_{Au} * \%v_{Au}}{\%w_{Au}} = \frac{\rho_{Au} * \left(\frac{\frac{\%w_{Au}}{\rho_{Au}}}{\frac{\%w_{Au}}{\rho_{Au}} + \frac{\%w_{CeOx}}{\rho_{CeOx}}} \right)}{\%w_{Au}}$$

$$\rho_{CeOx/npAu} = \frac{1}{\left(\frac{\%w_{Au}}{\rho_{Au}} + \frac{\%w_{CeOx}}{\rho_{CeOx}} \right)}$$

The specific surface area (S) and pore volume (V_p) can be obtained using the value of $\rho_{(CeOx/npAu)}$, Area3d and Volume3d of CeO_x/np-Au (Table 1), and the size correction factor:

$$S\ (m^2.{g_{CeOx/npAu}}^{-1}) = \frac{A_{CeOx/npAu}}{\rho_{CeOx/npAu} * V_{CeOx/npAu}} * \frac{\frac{1\ m^2}{10^{12}\mu m^2}}{\frac{1\ cm^3}{10^{12}\mu m^3}}$$

$$V_P(m^3.{g_{CeOx/npAu}}^{-1}) = \frac{V_{Pore}}{\rho_{CeOx/npAu} * V_{CeOx/npAu}} * \frac{\frac{1\ m^3}{10^{18}\mu m^3}}{\frac{1\ cm^3}{10^{12}\mu m^3}}$$

S8 - Estimated Spatial Resolution of Tomographic Imaging Techniques

The spatial resolution of the PXCT tomogram was estimated by Fourier shell correlation (FSC), as described previously.[3] For this purpose we computed two subtomograms, each of them using half the number of projections with double angular spacing, and we then computed the Fourier transform of each subtomogram. Figure S14 shows the FSC curve in blue, illustrating the correlation between the Fourier components from both subtomograms averaged in spherical shells in reciprocal space as a function of the spatial frequency. A spatial frequency of 1 corresponds to that of a single pixel, which is 13.3 nm. We then compared the FSC with the half-bit threshold, shown in red in Figure S14, which is analytically obtained for a signal-to-noise ratio of ~0.4 over the whole image, and has been proposed to be an appropriate threshold for comparing two subtomograms in tomography.[4] The point at which both curves intersect can be interpreted as the spatial frequencies that can be reproduced with sufficient

signal to noise ratio in the full 3D tomogram obtained from all projections, and this can then be considered an estimation of the isotropic 3D resolution of the full tomogram. In Figure S14 this point is at 0.59, corresponding to a half-period resolution of 22.6 nm.

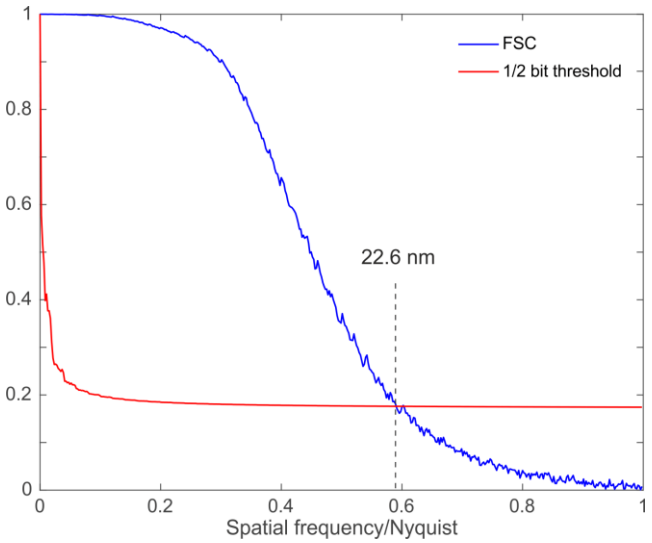

Figure S14. Estimation of the spatial resolution of PXCT by Fourier shell correlation.

S9 - Supplementary Movie Files

Movie files of the 3D renderings produced by PXCT, FIB-SEM-CT are included separately.

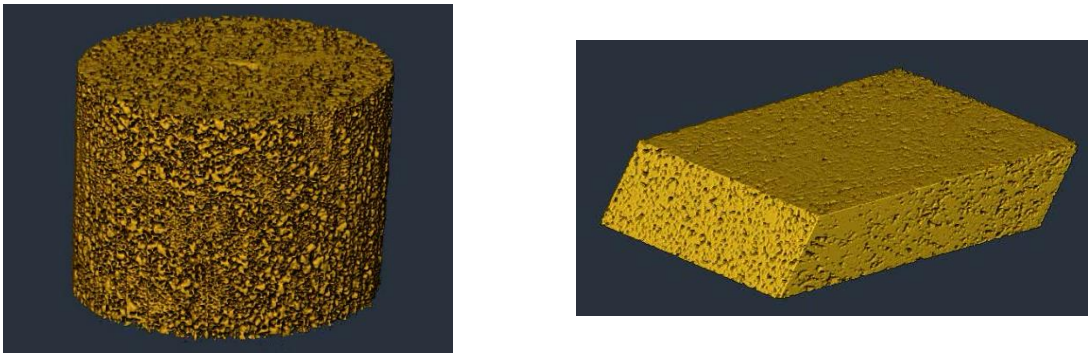

Figure S15. Snapshot from movie files showing PXCT data (left) and FIB-SEM-CT data (right).

References

[1] M. Holler, J. Raabe, R. Wepf, S. H. Shahmoradian, A. Diaz, B. Sarafimov, T. Lachat, H. Walther, M. Vitins, *Rev. Sci. Instrum.* **2017**, *88*, 113701
[2] H. Wadell, *J. Geol.* **1935**, *43*, 250.
[3] M. Holler, A. Diaz, M. Guizar-Sicairos, P. Karvinen, E. Färm, E. Härkönen, M. Ritala, A. Menzel, J. Raabe, O. Bunk, *Sci. Rep.* **2014**, *4*, 3857.
[4] M. van Heel, M. Schatz, *J. Struct. Biol.* **2005**, *151*, 250.